

Bounds on geometric wakefields in collimators and step transitions of arbitrary cross sections.

L. A. Shaposhnikov* and S. S. Baturin†

School of Physics and Engineering, ITMO University, St. Petersburg, Russia 197101

(Dated: December 18, 2023)

We present the wakefield conformal mapping technique that can be readily applied to the analysis of the radiation generated by an ultra-relativistic particle in the step transition and a collimator. We derive simple analytical expressions for the lower and upper bounds of both longitudinal and transverse wake potentials. We test the derived expressions against well-known formulas in several representative examples. The proposed method can greatly simplify the optimization of collimating sections, as well as become a useful tool in the shape optimization problems.

I. INTRODUCTION

When a relativistic charged particle passes near an inhomogeneity, it emits electromagnetic fields that inevitably interact with particles that follow the source of the radiation. Such interactions by radiation of different types are generalized into a convenient framework known as wakefield interactions [1, 2]. The analysis and computation of wakefields of various types - geometric, resistive wall [3], dielectric [4–6], and even metamaterial [7] - are the cornerstone of the design of any modern accelerator, be it a conventional machine like CLIC [8], ILC [9], LCLS-II [10] etc. or a wakefield accelerator like the A-STAR [11].

The wakefield generated in the transition of various components of the vacuum system (geometric wakes) and the related beam dynamics effects were among the first to be studied. Generally, these studies concentrated on particular geometries of the vacuum chambers and were initially restricted to circular cross sections. As accelerator technology advanced, researchers had to take into account more complex cross-sectional shapes, particularly in the design of the transition sections from the beam transport tube to the undulator in the case of X-FELs.

Geometric wakes may be essential for the design of modern collinear wakefield accelerators (CWAs). For example, in the A-STAR project [11, 12], when transitioning from a small aperture of the corrugated vacuum chamber [13] to the transition section [14], witness and driver beams may be significantly affected by wake influence, which could be reduced through proper optimization. Direct numerical treatment [15, 16] of this issue is the most accurate approach, yet optimization procedures for bunches with lengths of around $1 \mu\text{m}$ can be computationally expensive. Calculating the short-range wake requires a spatial mesh size that is a fraction of the bunch length, making submillimeter and micrometer-scale bunches a challenge.

A comprehensive study of geometric wakes within the optical approximation is considered in [17, 18], where sev-

eral exact analytical results on the wake potential (both longitudinal and transverse) have been obtained for step transitions, collimators and slits. While the approach of Ref.[17] provides a very powerful tool for the evaluation of geometric wakes, further improvement and simplification of this method are of additional value, especially in view of new possible applications to the CWA. In the present study, we follow the conformal mapping approach introduced in Refs.[19, 20] for the steady-state wake in structures of arbitrary cross sections. This method has proven useful in several advanced accelerator applications, such as flat beams Refs.[21, 22] and the recently introduced L-shape corrugated structure [23]. We start from the seminal idea of Heifets and Kheifets [24] for the circular collimator and combine it with the conformal mapping approach [20] and concepts of optical approximation of Ref.[17]. Based on the energy balance equation, we express the upper and lower bounds of the wake potential by the difference of the electromagnetic self-energy of the two-particle bunch in the incoming and outgoing beam pipes and independently arrive at the same cross-integral as in Ref.[17], which was derived using the indirect integration technique [25, 26]. We go one step further and evaluate this integral explicitly for the case of arbitrary cross sections of the collimator tubes. We show that upper and lower bounds for the exact Green's function for the longitudinal wake potential are expressed by a logarithm of the ratio of the corresponding conformal maps. The latter is a natural generalization of the well-known result for a round pipe. By means of the Panofsky-Wenzel theorem [27] we relate corresponding bounds on the Green's function for the transverse wake potential to the corresponding conformal maps and their derivatives. We conclude with a series of simple examples and transitions that reproduce known results.

* leon.shaposhnikov@metalab.ifmo.ru

† s.s.baturin@gmail.com

II. BASIC EQUATIONS

We consider the Maxwell system in CGS units in vacuum

$$\begin{aligned}\nabla \times \mathbf{E} &= -\frac{1}{c} \frac{\partial \mathbf{H}}{\partial t}, \\ \nabla \times \mathbf{H} &= \frac{4\pi}{c} \mathbf{j} + \frac{1}{c} \frac{\partial \mathbf{E}}{\partial t}, \\ \nabla \cdot \mathbf{E} &= 4\pi\rho, \\ \nabla \cdot \mathbf{H} &= 0.\end{aligned}\quad (1)$$

We assume that the particle is moving along the z -axis. In the ultra-relativistic limit the current produced by the particle and its charge density are connected through:

$$|\mathbf{j}| = j_z = c\rho(x, y, z - ct). \quad (2)$$

First, we introduce a new coordinate $\zeta = ct - z$ and split the Maxwell system into two parts:

$$\begin{aligned}[\nabla \times \mathbf{E}]_{\perp} &= -\frac{\partial \mathbf{H}_{\perp}}{\partial \zeta}, \\ [\nabla \times \mathbf{H}]_{\perp} &= \frac{\partial \mathbf{E}_{\perp}}{\partial \zeta};\end{aligned}\quad (3)$$

and

$$\begin{aligned}[\nabla \times \mathbf{E}]_z &= -\frac{\partial H_z}{\partial \zeta}, \\ [\nabla \times \mathbf{H}]_z &= 4\pi\rho + \frac{\partial E_z}{\partial \zeta}, \\ \nabla_{\perp} \cdot \mathbf{E}_{\perp} &= 4\pi\rho + \frac{\partial E_z}{\partial \zeta}, \\ \nabla_{\perp} \cdot \mathbf{H}_{\perp} &= \frac{\partial H_z}{\partial \zeta}.\end{aligned}\quad (4)$$

Here the \perp -symbol indicates field components orthogonal to the z -axis and ∇_{\perp} - is the nabla operator in the plane orthogonal to the z -axis.

Next, as in Ref.[20], we combine Eqs.(4) as

$$\begin{aligned}\nabla_{\perp} \cdot \mathbf{E}_{\perp} + i[\nabla \times \mathbf{E}]_z &= 4\pi\rho + \frac{\partial E_z}{\partial \zeta} - i\frac{\partial H_z}{\partial \zeta}, \\ \nabla_{\perp} \cdot \mathbf{H}_{\perp} + i[\nabla \times \mathbf{H}]_z &= i\left(4\pi\rho + \frac{\partial E_z}{\partial \zeta} - i\frac{\partial H_z}{\partial \zeta}\right).\end{aligned}\quad (5)$$

Finally, we introduce complex functions

$$\begin{aligned}e &= E_x + iE_y, \\ h &= H_x + iH_y,\end{aligned}\quad (6)$$

and note that ultra-relativistic particle inside a perfectly conducting pipe do not radiate, consequently $E_z = H_z = 0$ and the last terms in (5) vanish. Therefor, in complex notation of Eq.(6) one may reduce Eqs.(5) to

$$\frac{\partial e}{\partial \omega} = 2\pi\rho. \quad (7)$$

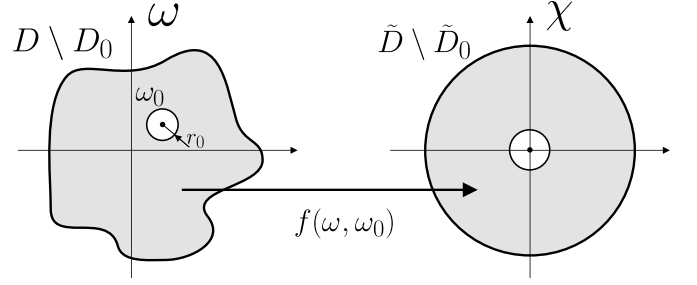


Figure 1. Action of the conformal map $f(\omega, \omega_0)$ that transforms area D into unit disk, while point ω_0 is mapped to the center of this disk.

Here $\omega = x + iy$. Since $h = ie$ (see Appendix B for details), we further consider only the equation for e . Eq.(7) must be supplemented with the boundary condition at a perfect conductor (PEC) that reads

$$\Re[e\tau^*] = 0. \quad (8)$$

Here, $\tau = \tau_x + i\tau_y$ is the tangential vector to the pipe surface in the cross section orthogonal to the z -axis, the asterisk represents the complex conjugation.

We introduce potential φ as

$$e = -2 \frac{\partial \varphi^*}{\partial \omega^*}. \quad (9)$$

It is apparent that φ is a solution to the 2D Poisson equation with the Dirichlet boundary condition on Γ_0 - the curve that encloses the vacuum channel of the pipe. We note that $\Delta_{\perp} = 4\partial_{\omega}\partial_{\omega}^*$ and write

$$\begin{aligned}\Delta_{\perp}\varphi &= -4\pi\rho, \\ \varphi|_{\Gamma_0} &= 0.\end{aligned}\quad (10)$$

Solution to the problem (10) above is well known (see for instance Refs.[28, 29]) and reads

$$\varphi = -2 \int dx_0 dy_0 \rho(x_0, y_0, \zeta) \ln |f(\omega, \omega_0)|. \quad (11)$$

Here, $f(\omega, \omega_0)$ is the conformal mapping function that gives the mapping of the D -region onto a disk such that the point ω_0 is mapped to the center of a disk. The electric field is recovered with the help of Eq.(9) and reads

$$e = 2 \int dx_0 dy_0 \rho(x_0, y_0, \zeta) \left[\frac{f'(\omega, \omega_0)}{f(\omega, \omega_0)} \right]^*, \quad (12)$$

where the prime symbol denotes the derivative by ω .

III. ENERGY EVALUATION

We start from the energy balance equation

$$-\frac{\partial}{\partial t} \int_V w dV = \int_{\partial V} \mathbf{S} \cdot d\mathbf{A} + \int_V \mathbf{j} \cdot \mathbf{E} dV. \quad (13)$$

We assume that the total energy $W = \int_V w dV$ is conserved. This implies that

$$W(t = -\infty) = W(t = \infty). \quad (14)$$

The beam and the radiation travels along the z axis, consequently only z -component of the Poynting's vector does not vanish. After integrating Eq.(13) over time and accounting for the condition Eq.(14) we get

$$\begin{aligned} & \int_{-\infty}^{\infty} \int_{D_A} S_z dx dy dt + \int_{-\infty}^{\infty} \int_{D_B} S_z dx dy dt \\ & + \int_{-\infty}^{\infty} \int_V j_z E_z dV dt = 0. \end{aligned} \quad (15)$$

The last term is the energy lost/gained by the bunch due to the interaction U_{rad} and the first two terms are the total fluxes Φ_A and Φ_B though the cross sections D_A and D_B correspondingly.

The flux though the cross section A consists of the incoming flux of the source and outgoing flux of the scattered field. The flux through the cross section B includes the outgoing flux of the source and the remaining part of the scattered field flux. With the help of Eq.(6) one may write for the Poynting vectors of the source

$$S_z = \frac{c}{4\pi} [\mathbf{E} \times \mathbf{H}]_z = \frac{c}{4\pi} \Im[e^* h] \quad (16)$$

Recalling the connection $h = ie$ we get

$$S_z = \frac{c}{4\pi} |e|^2, \quad (17)$$

and thus

$$\Phi_{A,B}^{\text{sl}} = \frac{c}{4\pi} \int_{-\infty}^{\infty} \int_{D_{A,B}} |e|^2 dx dy dt. \quad (18)$$

It is convenient to rewrite Eq.(15) as

$$U_{\text{rad}} = -\Phi_B^{\text{sl}} + \Phi_A^{\text{sl}} - \Phi^{\text{scat}}, \quad (19)$$

where we have accounted for the sign of the fluxes and introduced Φ^{scat} - the total flux of the scattered field (though both the cross section D_A and D_B . The normal vector is pointed inside the volume enclosed by the beam pipes and cross sections A and B . Negative sign in-front of the scattered field flux accounts for the fact that the scattered field propagates outside the volume and fluxes through both cross sections A and B are negative. Eq.(19) can be used right away to estimate the energy gain in the step-in transition. Replacing cross

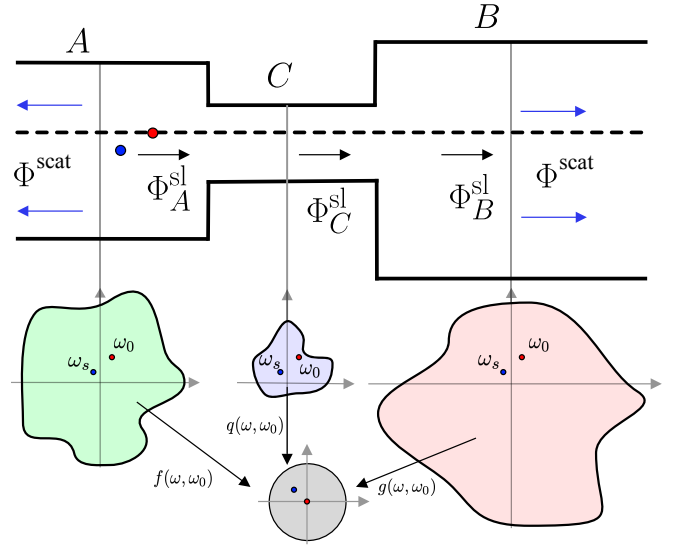


Figure 2. Sketch of the arbitrary step collimator.

section B with cross section C (see Fig.2) in Eq.(19) we get the upper bound for the energy gain $U_{\text{rad}}^{\text{s,in}}$ in the pure step-in transition.

$$U_{\text{rad}}^{\text{s,in}} < \Phi_A^{\text{sl}} - \Phi_C^{\text{sl}}, \quad (20)$$

a known phenomenon (see for instance Ref.[24]). It should be noted that the flux Φ^{scat} satisfies the same inequality as follows from Eq.(19) under the assumption $U_{\text{rad}} > 0$, namely,

$$\Phi_{\text{s,in}}^{\text{scat}} < \Phi_A^{\text{sl}} - \Phi_C^{\text{sl}}. \quad (21)$$

One of the important observations made in Ref.[24] is that Φ^{scat} is the same for both step-in and step-out transition of the same configuration. This is a direct consequence of the parity-time symmetry of the problem and the application of the Lorentz reciprocity theorem. Thus, following Ref.[24] we may write for the step-out

$$\Phi_{\text{s,out}}^{\text{scat}} < \Phi_B^{\text{sl}} - \Phi_C^{\text{sl}}. \quad (22)$$

To get the estimate for the upper bound of the energy loss we account for Eq.(21), Eq.(22) and note that the total flux Φ^{scat} for the collimator is the sum of step-in and step-out fluxes. Consequently, we have

$$\Phi^{\text{scat}} = \Phi_{\text{s,in}}^{\text{scat}} + \Phi_{\text{s,out}}^{\text{scat}} < \Phi_A^{\text{sl}} + \Phi_B^{\text{sl}} - 2\Phi_C^{\text{sl}}. \quad (23)$$

Under the assumption of $U_{\text{rad}} < 0$ in a collimator and combining Eq.(23) with Eq.(19) we get

$$|U_{\text{rad}}| < 2\Phi_B^{\text{sl}} - 2\Phi_C^{\text{sl}}. \quad (24)$$

We note that provided upper bound rapidly approaches the exact value for the $|U_{\text{rad}}|$ when conditions of the optical approximation are met:

$$\lambda \ll b, l \ll \frac{b^2}{\lambda}. \quad (25)$$

Here λ is the reduced wavelength of the radiation, l is the length of an obstacle, and b is the minimal cross section size of the beam pipe.

The first condition indicates that the obstacle must be much larger than the reduced wavelength of the radiation. The second condition requires the object to be short compared to the catch-up distance. More information on the optical approximation can be found in Ref.[17]. We note that for the short bunches this approximation provides good quantity agreement between analytical results and simulations [17, 18, 24].

Dropping Φ^{scat} in Eq.(19) on can get the lower bound for the $|U_{\text{rad}}|$, that we combine with Eq.(24) and finally get

$$\Phi_B^{\text{sl}} - \Phi_A^{\text{sl}} < |U_{\text{rad}}| < 2\Phi_B^{\text{sl}} - 2\Phi_C^{\text{sl}}. \quad (26)$$

We point out that both bounds are firm and valid regardless of the approximation and are derived from the estimates on Φ^{scat} , however, both bounds hold only if one knows for a fact that the beam experiences net energy loss when passing through a collimator.

Thus, the lower and upper bounds for the energy loss in a collimator transition can be estimated using the differences of the charge self-energies calculated in different cross sections.

It is worth pointing out that if the scattered energy is dissipated or trapped inside the volume, then an additional energy term that effectively decreases the scattered field flux must be accounted for, this, however, does not affect the upper bound and the inequality given by Eq.(26) remains valid.

IV. LOSS FACTOR AND WAKE POTENTIAL

A. Loss factor of a single short bunch

We start from a single, short $\sigma_z \ll a$ (where a - is the characteristic size of the smallest aperture), pencil-like Gaussian bunch

$$\rho(x, y, \zeta) = Q \frac{\delta(x - x_0) \delta(y - y_0)}{\sqrt{2\pi}\sigma_z} \exp\left[-\frac{\zeta^2}{2\sigma_z^2}\right]. \quad (27)$$

Here, Q is the total charge and σ_z is the RMS bunch length. By plugging Eq.(27) into the Eq.(12) we get

$$e = 2Q \frac{\exp\left[-\frac{\zeta^2}{2\sigma_z^2}\right]}{\sqrt{2\pi}\sigma_z} \left[\frac{f'(\omega, \omega_0)}{f(\omega, \omega_0)} \right]^*, \quad (28)$$

with $\omega_0 = x_0 + iy_0$. With the help of the Eq.(27) from Eq.(18) we get

$$\Phi_{B,A}^{\text{sl}} = \frac{4Q^2}{4\pi} \int_{-\infty}^{\infty} cdt \frac{\exp\left[-\frac{\zeta^2}{\sigma_z^2}\right]}{2\pi\sigma_z^2} \times \int_{D_{A,B}} \frac{|f'(\omega, \omega_0)|^2}{|f(\omega, \omega_0)|^2} dxdy \quad (29)$$

The first integral in Eq.(29) with $d\zeta = cdt$ evaluates to

$$\int_{-\infty}^{\infty} d\zeta \frac{\exp\left[-\frac{\zeta^2}{\sigma_z^2}\right]}{2\pi\sigma_z^2} = \frac{1}{2\sigma_z\sqrt{\pi}}. \quad (30)$$

The second integral over $D_{A,B}$ does not converge at the lower limit. To eliminate this divergence, we cut out the circle of the infinitesimally small radius r_0 with the center in the ω_0 , we call this area D_0 . Next, we integrate over $D_{A,B} \setminus D_0$.

We recall that switching from ω to $\chi = f(\omega, \omega_0) = \tilde{x} + i\tilde{y}$ (see Fig.II) results in the Jacobian in the transformation of the elementary square: $d\tilde{x}d\tilde{y} = |f'(\omega, \omega_0)|^2 dxdy$. Boundaries $\partial\tilde{D}_{A,B}$ and the boundary of the cut circle $\partial\tilde{D}_0$ in the χ plane are defined as

$$\begin{aligned} \partial\tilde{D}_{A,B} &= \{\tilde{\mathbf{r}} \mid |\tilde{\mathbf{r}}| = 1\}, \\ \partial\tilde{D}_0 &= \{\tilde{\mathbf{r}} \mid \forall \varphi : f(\omega_0 + r_0 e^{i\varphi}, \omega_0)\}. \end{aligned} \quad (31)$$

We assume that r_0 is much smaller than any other characteristic size in our problem. Thus, we expand $f(\omega_0 + r_0 e^{i\varphi}, \omega_0) \approx f(\omega_0, \omega_0) + f'(\omega_0, \omega_0) r_0 e^{i\varphi} = f'(\omega_0, \omega_0) r_0 e^{i\varphi}$. With this we can define \tilde{D}_0 as a disk with radius $r_0 |f'(\omega_0, \omega_0)|$ centered at the point 0:

$$\partial\tilde{D}_0 = \{\tilde{\mathbf{r}} \mid |\tilde{\mathbf{r}}| = r_0 |f'(\omega_0, \omega_0)|\}. \quad (32)$$

In the χ plane where $\tilde{D}_{A,B}$ is now a disk and the last integral in Eq.(29) can be easily evaluated. If f is the mapping of the D_A onto a unit disk we get

$$\begin{aligned} \int_{D_A \setminus D_0} \left| \frac{f'(\omega, \omega_0)}{f(\omega, \omega_0)} \right|^2 dxdy &= \int_{\tilde{D}_A \setminus \tilde{D}_0} \frac{1}{|f(\omega, \omega_0)|^2} d\tilde{x}d\tilde{y} = \\ &= \int_{r_0 |f'(\omega_0, \omega_0)|}^1 \frac{2\pi}{\tilde{r}} d\tilde{r} = -2\pi \ln(r_0 |f'(\omega_0, \omega_0)|). \end{aligned} \quad (33)$$

If now $g(\omega, \omega_0)$ is the mapping of the area D_B the cross section of the outgoing pipe onto the unit disk such that ω_0 - the transverse position of the pencil beam is mapped

to the center of the disk we get

$$\int_{D_B \setminus D_0} \left| \frac{g'(\omega, \omega_0)}{g(\omega, \omega_0)} \right|^2 dxdy = \int_{D'_B \setminus D'_0} \frac{1}{|g(\omega, \omega_0)|^2} d\tilde{x}d\tilde{y} = \int_{r_0|g'(\omega, \omega_0)|}^1 \frac{2\pi}{\tilde{r}} d\tilde{r} = -2\pi \ln(r_0 |g'(\omega_0, \omega_0)|). \quad (34)$$

From Eq.(26) combining Eq.(29), Eq.(30), Eq.(33) and Eq.(34) we evaluate the lower bound for the energy loss as:

$$|U_{\text{rad}}| > \frac{1}{2\sigma_z \sqrt{\pi}} \frac{Q^2}{2} 4 \ln \left| \frac{f'(\omega_0, \omega_0)}{g'(\omega_0, \omega_0)} \right|. \quad (35)$$

The loss factor $\kappa_{\parallel} = |U_{\text{rad}}|/Q^2$ is then

$$\kappa_{\parallel} > \frac{1}{2\sigma_z \sqrt{\pi}} \frac{1}{2} 4 \ln \left| \frac{f'(\omega_0, \omega_0)}{g'(\omega_0, \omega_0)} \right|. \quad (36)$$

we observe that we recover familiar logarithmic term. Yet, the form of this term is now more general and accounts for the form factors of the corresponding pipes.

We note the factor 1/2 in both Eq.(36) and Eq.(35). Next, we consider a symmetric transition (when the incoming and outgoing pipes have the same cross section). We introduce a conformal mapping function $q(\omega, \omega_0)$, which maps the cross section C of the central part of the collimator onto a unit disk in such a way that the point of the particle ω_0 is mapped onto the center of the disk. With the help of Eq.(26) we arrive at a generalization of the formula for the loss factor of the arbitrary step collimator:

$$\kappa_{\parallel}^{\text{col}} < \frac{1}{2\sigma_z \sqrt{\pi}} 4 \ln \left| \frac{f'(\omega_0, \omega_0)}{q'(\omega_0, \omega_0)} \right|. \quad (37)$$

Using the inequality Eq.(26), the generalized formula for the beam with the longitudinal charge distribution $\rho_{\parallel}(s)$ passing through a three-pipe junction (a full step in and a full step out)

$$\begin{aligned} \kappa_{\parallel} &> 2 \|\rho_{\parallel}(s)\|_{L^2}^2 \ln \left| \frac{f'(\omega_0, \omega_0)}{g'(\omega_0, \omega_0)} \right|, \\ \kappa_{\parallel} &< 4 \|\rho_{\parallel}(s)\|_{L^2}^2 \ln \left| \frac{q'(\omega_0, \omega_0)}{g'(\omega_0, \omega_0)} \right|. \end{aligned} \quad (38)$$

Where $\|\rho_{\parallel}(s)\|_{L^2}^2$ is the square of the L^2 norm of the longitudinal bunch distribution and is given by

$$\|\rho_{\parallel}(s)\|_{L^2}^2 = \int_{-\infty}^{\infty} |\rho_{\parallel}(s)|^2 ds. \quad (39)$$

B. Green's function and wake potential

In this section we derive a two-point function and relate it to the wake potential. We extend our analysis to

the general case of two particles, one traveling behind the other at a distance s .

The charge density in this case is

$$\rho = \rho_1 + \rho_2 = Q_1 \delta(x - x_0) \delta(y - y_0) \delta(\zeta) + Q_2 \delta(x - x_s) \delta(y - y_s) \delta(\zeta - s). \quad (40)$$

With the help of Eq.(40) and Eq.(12) we get

$$\begin{aligned} e = e_1 + e_2 &= Q_1 \delta(\zeta) \left[\frac{f'(\omega, \omega_0)}{f(\omega, \omega_0)} \right]^* + \\ &+ Q_2 \delta(\zeta - s) \left[\frac{f'(\omega, \omega_s)}{f(\omega, \omega_s)} \right]^*, \end{aligned} \quad (41)$$

where $Q_1 + Q_2 = Q$ - the total charge of the two-particle bunch.

We substitute Eq.(40) and Eq.(41) into the Eq.(15) and get

$$\begin{aligned} cQ_1 \int_{-\infty}^{\infty} E_z(x_0, y_0, z = ct, t) dt + \\ + cQ_2 \int_{-\infty}^{\infty} E_z(x_s, y_s, z = ct - s, t) dt &= -\Phi_B^G + \Phi_A^G - \Phi_A^{\text{ref}}. \end{aligned} \quad (42)$$

With $\Phi_{A,B}^G$ given by

$$\begin{aligned} \Phi_{A,B}^G &= \frac{c}{4\pi} \int_{-\infty}^{\infty} \int_{D_A, D_B} |e_1|^2 dxdydt + \\ &+ \frac{c}{4\pi} \int_{-\infty}^{\infty} \int_{D_A, D_B} |e_2|^2 dxdydt + \\ &+ \frac{c}{4\pi} \int_{-\infty}^{\infty} \int_{D_A, D_B} (e_1 e_2^* + e_2 e_1^*) dxdydt. \end{aligned} \quad (43)$$

The first two terms correspond to the self interaction of each particle as was discussed in Sec.IV A. The right-hand side of the energy balance equation (42) consists of three terms the first term due to the causality (the longitudinal field created by the second particle at the position of the first particle is zero $E_{2,z} = 0$) is just the loss of the first particle to the radiation

$$U_{\text{rad}}^{(1)} = cQ_1 \int_{-\infty}^{\infty} E_{1,z}(x_0, y_0, z = ct, t) dt. \quad (44)$$

The second term in Eq.(42) due to the superposition principle

$$\begin{aligned} E_z(x_s, y_s, z = ct - s, t) &= \\ E_{1,z}(x_s, y_s, z = ct - s, t) + E_{2,z}(x_s, y_s, z = ct - s, t) \end{aligned} \quad (45)$$

is the sum of the losses of the second particle to the radiation

$$U_{\text{rad}}^{(2)} = cQ_1 \int_{-\infty}^{\infty} E_{2,z}(x_0, y_0, z = ct, t) dt. \quad (46)$$

and a wake field interaction term

$$cQ_2 \int_{-\infty}^{\infty} E_{1,z}(x_s, y_s, z = ct - s, t) dt = -cQ_1 Q_2 w_{\parallel}(s). \quad (47)$$

Here $w_{\parallel}(s)$ is the longitudinal wake potential.

As before, assuming $U_{\text{rad}}^{(1,2)} < 0$ and considering the inequality Eq.(26) the following inequality for the wake potential is obtained

$$\phi_B^{\text{cr}} - \phi_A^{\text{cr}} < w(s) < 2\phi_B^{\text{cr}} - 2\phi_C^{\text{cr}}, \quad (48)$$

with ϕ^{cr} being the normalized “cross” flux though the corresponding cross section

$$\phi_{A,B,C}^{\text{cr}} = \frac{1}{4\pi} \int_{-\infty}^{\infty} \int_{D_A, D_B, D_C} \frac{e_1 e_2^* + e_2 e_1^*}{Q_1 Q_2} dx dy dt. \quad (49)$$

We note that the expression for the “cross”-flux is in full agreement with the one from Ref.[17]

With the help of Eq.(41) we evaluate the integral over t and obtain for the cross section A

$$\phi_A^{\text{cr}} = \frac{\delta(s)}{\pi} I_A. \quad (50)$$

Here I_A is an exchange integral that reads:

$$I_A = 2 \int_{D_A} \Re \left\{ \left[\frac{f'(\omega, \omega_0)}{f(\omega, \omega_0)} \right]^* \left[\frac{f'(\omega, \omega_s)}{f(\omega, \omega_s)} \right] \right\} dx dy. \quad (51)$$

The integral can be evaluated explicitly (see Appendix A for the details) and reads

$$I_A = -\pi \{ \ln [f(\omega_0, \omega_s)] + \ln [f(\omega_s, \omega_0)] \}. \quad (52)$$

Expression above for the integral can be simplified further to

$$I_A = -2\pi \ln |f(\omega_s, \omega_0)|. \quad (53)$$

Combining Eq.(48) with Eq.(50) and accounting for the Eq.(53) we get

$$\begin{aligned} w_{\parallel}(s) &> 2\delta(s) \ln \left| \frac{f(\omega_s, \omega_0)}{g(\omega_s, \omega_0)} \right|, \\ w_{\parallel}(s) &< 4\delta(s) \ln \left| \frac{q(\omega_s, \omega_0)}{g(\omega_s, \omega_0)} \right|. \end{aligned} \quad (54)$$

Here, as before, the function g - is the conformal mapping of the cross section D_B onto a unit disk, and function q - is the conformal mapping of the cross section D_C onto a unit disk. In all cases, the index 0 corresponds to the leading particle and the index s to the trailing particle.

Transverse wake potential is recovered from Eq.(54) with the help of the Panofsky-Wenzel theorem [27]

$$\partial_s \vec{w}_{\perp} = \nabla_{\perp} w_{\parallel}. \quad (55)$$

In the complex notations equations above reads

$$\partial_s w_{\perp}^* = 2\partial_{\omega_s} w_{\parallel}, \quad (56)$$

where $w_{\perp} = w_x + iw_y$. Combining Eq.(54) and (56) we arrive at the estimates for the transverse wake potential in a form

$$\begin{aligned} |w_x(s)| &> 2\theta(s) \left| \Re \left\{ \left[\frac{f'(\omega_s, \omega_0)}{f(\omega_s, \omega_0)} - \frac{g'(\omega_s, \omega_0)}{g(\omega_s, \omega_0)} \right] \right\} \right|, \\ |w_y(s)| &> 2\theta(s) \left| \Im \left\{ \left[\frac{f'(\omega_s, \omega_0)}{f(\omega_s, \omega_0)} - \frac{g'(\omega_s, \omega_0)}{g(\omega_s, \omega_0)} \right] \right\} \right|, \\ |w_x(s)| &< 4\theta(s) \left| \Re \left\{ \left[\frac{q'(\omega_s, \omega_0)}{q(\omega_s, \omega_0)} - \frac{g'(\omega_s, \omega_0)}{g(\omega_s, \omega_0)} \right] \right\} \right|, \\ |w_y(s)| &< 4\theta(s) \left| \Im \left\{ \left[\frac{q'(\omega_s, \omega_0)}{q(\omega_s, \omega_0)} - \frac{g'(\omega_s, \omega_0)}{g(\omega_s, \omega_0)} \right] \right\} \right|. \end{aligned} \quad (57)$$

Here $\theta(s)$ is the Heaviside step-function.

Note that the lower and the upper bounds always have the same sign, so the sign of the wake is fixed by the sign of the corresponding upper bound, which means that the function $\frac{q'(\omega_s, \omega_0)}{q(\omega_s, \omega_0)} - \frac{g'(\omega_s, \omega_0)}{g(\omega_s, \omega_0)}$ gives the structure of the transverse wake potential. This fact can be used to construct a two-dimensional kick map estimate based solely on the complex derivative of the upper bound in Eq.(54). Thus, we introduce a bounding transverse wake potential of the form

$$\mathcal{W}_{\perp}(s)^* = 4\theta(s) \left[\frac{q'(\omega_s, \omega_0)}{q(\omega_s, \omega_0)} - \frac{g'(\omega_s, \omega_0)}{g(\omega_s, \omega_0)} \right]. \quad (58)$$

The above expression makes it possible to estimate the maximum amplitude and the structure of the transverse wake potential at the same time.

V. EXAMPLES

In this section, we consider two basic conformal maps and apply them to evaluate the wake potential for round-to-round, flat-to-flat, and flat-to-round step-out transitions.

A. Conformal maps

The conformal map $f_{c(a)}(\omega, \omega_i)$ of a disk (see Fig.3 left part of the diagram) with radius a onto a unit disk such

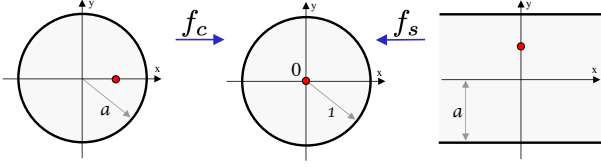


Figure 3. Diagrams of conformal mappings. Displaced disk on a unit disk (left part of the diagram) and strip parallel to the x -axis on a unit disk (right part of the diagram).

that the point of a source ω_0 is mapped to the center of a unit disk is given by [28, 29]

$$f_c(\omega, \omega_0) = a \frac{\omega - \omega_0}{a^2 - \omega \omega_0} \quad (59)$$

A function $F(\omega)$, which maps an infinite parallel to the y -axis strip with the height $2a$ to a disk of radius a is given by [28, 29]:

$$F(\omega) = a \tan \left[\frac{\pi}{4a} \omega \right]. \quad (60)$$

Combining (59) and (60) we arrive at the map for the strip onto a unit disk with the point ω_0 mapped to the center of the unit disk

$$f(\omega, \omega_0) = \frac{\tan \left(\frac{\pi}{4} \frac{\omega}{a} \right) - \tan \left(\frac{\pi}{4} \frac{\omega_0}{a} \right)}{1 - \tan \left(\frac{\pi}{4} \frac{\omega}{a} \right) \tan \left(\frac{\pi}{4} \frac{\omega_0}{a} \right)}. \quad (61)$$

Substitution $\omega \rightarrow i\omega^*$ makes the strip parallel to the x -axis (see Ref.[21]) and we finally get (see Fig.3 right part of the diagram)

$$f_{s(a)}(\omega, \omega_0) = i \frac{\tanh \left(\frac{\pi}{4} \frac{\omega^*}{a} \right) - \tanh \left(\frac{\pi}{4} \frac{\omega_0^*}{a} \right)}{1 - \tanh \left(\frac{\pi}{4} \frac{\omega^*}{a} \right) \tanh \left(\frac{\pi}{4} \frac{\omega_0^*}{a} \right)}. \quad (62)$$

B. Step-out transitions

We assume that the cross sections of the incoming waveguide and the collimating section are equal $D_C \equiv D_B$ ($q \equiv g$). Such a transition is called step-out.

For the step-out transition as well as for the collimator with such a step-out transition, the upper bound of the longitudinal wake potential is given by Eq.(54) and the transverse wake potential can be estimated using Eq.(58).

1. Round to round transition

We examine the transition between two round pipes with radii a_1 and a_2 respectively (Fig.4a), the symmetry axis of the first (incoming) pipe is at the point $\omega = \omega_c$, and the symmetry axis of the second (outgoing) pipe is at $\omega = 0$. Since we are studying a step-out transition, we

introduce a constraint on the pipe parameters: $|\omega_c| + a_1 < a_2$. The cross section of the transition is sketched in Fig.4(a).

With the help of Eq.(59) we calculate the conformal maps q and g :

$$q = f_{c(a_1)}(\omega - \omega_c, \omega_{0,s} - \omega_c) = \quad (63)$$

$$\frac{a_1(\omega - \omega_{0,s})}{a_1^2 - (\omega - \omega_c)(\omega_{0,s}^* - \omega_c^*)},$$

$$g = f_{c(a_2)}(\omega, \omega_{0,s}) = \frac{a_2(\omega - \omega_{0,s})}{a_2^2 - \omega \omega_{0,s}^*}. \quad (64)$$

We combine Eq.(63) and Eq.(54), and arrive at the upper bound for the wake potential in the form:

$$w_{\parallel} < 4\delta(s) \ln \left| \frac{a_1}{a_2} \frac{a_2^2 - \omega_{0,s}^* \omega_s}{a_2^2 - (\omega_s - \omega_c)(\omega_0^* - \omega_c^*)} \right|. \quad (65)$$

In the trivial case, when both waveguides and particles are aligned to the symmetry axis ($\omega_c = \omega_0 = \omega_s = 0$) Eq.(65) simplifies to a well known expression [18, 24]

$$w_{\parallel} < 4\delta(s) \ln \frac{a_2}{a_1}. \quad (66)$$

If we consider a slightly misaligned waveguide ($\omega_c \ll a_1$) and a small displacement of both particles from the origin ($|\omega_{0,s}| \ll a_1$), then the Taylor expansion to the lowest order in $|\omega_{0,c}|$ of the Eq.(65) reads:

$$w_{\parallel} = 4\delta(s) \ln \left| \frac{a_2}{a_1} - \frac{a_2 |\omega_0| |\omega_c|}{a_1^3} \cos(\phi_0 - \phi_c) \right|. \quad (67)$$

For the transverse wake potential with the help of the Eq.(58) and Eqs.(63) we get

$$\mathcal{W}_{\perp}^*(s) = 4\theta(s) \left\{ \frac{\omega_0^* [a_2^2 - a_1^2 - \omega_c \omega_0^*] - \omega_c^* [a_2^2 - \omega_c \omega_0^*]}{[a_2^2 - \omega_s \omega_0^*] [a_1^2 - (\omega_s - \omega_c)(\omega_0^* - \omega_c^*)]} \right\}. \quad (68)$$

Assuming $\omega_c = 0$ and $\omega_s = \omega_0 \ll a_{1,2}$ we recover a known formula derived in Ref.[30].

$$\mathcal{W}_{\perp}(s) = 4\theta(s) \omega_0 \left[\frac{1}{a_1^2} - \frac{1}{a_2^2} \right]. \quad (69)$$

2. Planar to planar transition

Next we consider a transition from a planar aperture with half the gap a_1 to a planar aperture with half the gap a_2 . As before $a_2 > a_1$. The cross section of the transition is shown in Fig.4b.

Simplification of the Eq.(62) gives

$$q = f_{s(a_1)} = i \frac{\sinh \left[\frac{\pi}{4} \frac{x - i(y - y_0)}{a_1} \right]}{\cosh \left[\frac{\pi}{4} \frac{x - i(y + y_0)}{a_1} \right]}, \quad (70)$$

$$g = f_{s(a_2)} = i \frac{\sinh \left[\frac{\pi}{4} \frac{x - i(y - y_0)}{a_2} \right]}{\cosh \left[\frac{\pi}{4} \frac{x - i(y + y_0)}{a_2} \right]}.$$

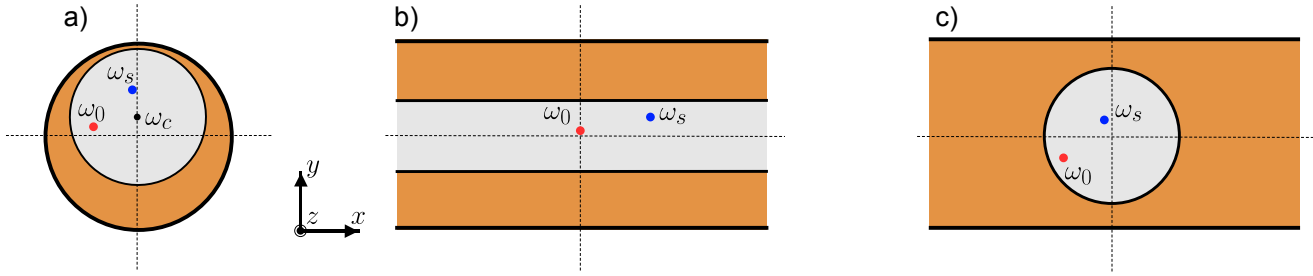


Figure 4. Sketches of the several transitions that was examined. Orange area corresponds to the cross section of the “out” waveguide, and light grey to the cross section of the “in” waveguide. The red dots are for the source particle, the blue dots are for the test particle, and the point ω_c corresponds to the center of the incoming pipe.

Above, we assumed that without the loss of generality $\omega_0 = iy_0$ and $\omega_s = x + iy$. We combine Eq.(54) and Eq.(70) and arrive at the expression for the upper bound on the w_{\parallel} in the form

$$w_{\parallel} < 4\delta(s) \times \ln \left| \frac{\sinh \left[\frac{\pi}{4} \frac{x-i(y-y_0)}{a_1} \right]}{\cosh \left[\frac{\pi}{4} \frac{x-i(y+y_0)}{a_1} \right]} \frac{\cosh \left[\frac{\pi}{4} \frac{x-i(y+y_0)}{a_2} \right]}{\sinh \left[\frac{\pi}{4} \frac{x-i(y-y_0)}{a_2} \right]} \right|. \quad (71)$$

If both particles are at the origin $\omega_s = \omega_0 = 0$ we recover a known result [18] that coincides with Eq.(66)

$$w_{\parallel} < 4\delta(s) \ln \frac{a_2}{a_1}. \quad (72)$$

The transverse wake potential is calculated based on the Eq.(58) and Eqs.(70). After some algebra we arrive at

$$\mathcal{W}_{\perp}^*(s) = \frac{4\theta(s)i\pi \cos \left[\frac{\pi y_0}{2a_1} \right]}{2a_1 \sin \left[\frac{\pi y_0}{2a_1} \right] + 2ia_1 \sinh \left[\frac{\pi}{2a_1} (x + iy) \right]} - \frac{4\theta(s)i\pi \cos \left[\frac{\pi y_0}{2a_2} \right]}{2a_2 \sin \left[\frac{\pi y_0}{2a_2} \right] + 2ia_2 \sinh \left[\frac{\pi}{2a_2} (x + iy) \right]}. \quad (73)$$

Assuming $x = 0$ and $y \ll a_{1,2}$ and $y_0 \ll a_{1,2}$ we get

$$\mathcal{W}_y(s) = 4\theta(s) \frac{\pi^2}{4} \left[\frac{y}{6} + \frac{y_0}{3} \right] \left[\frac{1}{a_1^2} - \frac{1}{a_2^2} \right]. \quad (74)$$

For a special case of $y = y_0$, we arrive at the following expression

$$\mathcal{W}_y(s) = 4\theta(s) \frac{\pi^2}{8} y_0 \left[\frac{1}{a_1^2} - \frac{1}{a_2^2} \right], \quad (75)$$

that differs from the Eq.(69) by a factor of $\pi^2/8$.

3. Round to planar transition

Finally, consider the transition from the pipe with radius a_1 centered at the origin to the planar waveguide of an aperture $2a_2$ (Fig.4c). We assume $a_1 < a_2$.

With the help of the Eq.(59) and Eq.(62), we calculate conformal maps q and g :

$$q = f_{c(a_1)}(\omega, \omega_{0,s}) = \frac{a_1(\omega - \omega_{0,s})}{a_1^2 - \omega\omega_{0,s}^*}, \quad (76)$$

$$g = f_{s(a_2)}(\omega, \omega_{0,s}) = i \frac{\tanh \left(\frac{\pi}{4} \frac{\omega^*}{a_2} \right) - \tanh \left(\frac{\pi}{4} \frac{\omega_{0,s}^*}{a_2} \right)}{1 - \tanh \left(\frac{\pi}{4} \frac{\omega^*}{a_2} \right) \tanh \left(\frac{\pi}{4} \frac{\omega_{0,s}}{a_2} \right)}. \quad (77)$$

Substituting Eq.(76) into Eq.(54) and proceeding to the limit $\omega_s = \omega_0 = 0$ we get

$$w_{\parallel} < 4\delta(s) \ln \left[\frac{4}{\pi} \frac{a_2}{a_1} \right]. \quad (78)$$

We note that along with the familiar term $\ln \frac{a_2}{a_1}$ as in eq.(66) we get an additional $\ln \frac{4}{\pi}$ - a form factor mismatch contribution. Note that geometry mismatch tends to increase the losses.

Substituting $\omega_0 = x_0 + iy_0$ and $\omega_s = x + iy$ into Eq.(76) with the help of Eq.(55) and Eq.(54) we get

$$\mathcal{W}_x(s) = 4\theta(s) \frac{x_0}{a_1^2}, \quad (79)$$

$$\mathcal{W}_y(s) = 4\theta(s) \frac{y_0}{a_1^2} \left[1 - \frac{\pi^2}{8} \frac{a_1^2}{a_2^2} \right].$$

Here we have assumed $y = y_0$ and $x = x_0$ in the final expression for a lowest-order Taylor decomposition. Note that the transverse wake has the same structure as in the round-to-round and planar-to-planar cases and consists of a difference of the inverse squares of the corresponding characteristic sizes in the corresponding direction. Each characteristic size is multiplied by a corresponding form factor. For the \mathcal{W}_y it is the same as for the planar case - $\pi^2/8$. For \mathcal{W}_x , the x parameter of the planar structure is ∞ , and only the first term survives.

Interestingly, if $a_2^2 = \pi^2/8a_1^2$ the y component of the transverse wake potential vanishes $\mathcal{W}_y = 0$. Furthermore, if $a_1^2 < a_2^2 < \pi^2/8a_1^2$ we get $\mathcal{W}_y < 0$ and the wake is focusing. The maximum focusing strength is at $a_1 = a_2$

$$\mathcal{W}_y(s) < -4\theta(s) \frac{y_0}{a_1^2} \left[\frac{\pi^2}{8} - 1 \right] \approx -0.93\theta(s) \frac{y_0}{a_1^2}. \quad (80)$$

We can see that the strength of the focusing force is about 1/4 of the kick in the x direction.

VI. CONCLUSION

We have revised the evaluation of the geometric wake potential in the collimators and step transitions with perfectly conducting walls. Building on the model and ideas of Ref.[24] and Ref.[20], we demonstrated that the wake potential can be well estimated using the conformal mapping technique. In the case where the cross sections of the incoming collimating and outgoing pipes have simple shapes (rectangular, slab, circular, elliptical), the mapping is evaluated explicitly. This in turn allows convenient analytical calculation of the corresponding form factors for both longitudinal and transverse wake potentials. If the cross section is an arbitrary single connected region, the corresponding map and its derivative can be numerically evaluated using the Zipper algorithm [31]. Zipper allows fast and accurate evaluation of the conformal mapping, but more importantly, it can produce the derivative of the mapping along with the map without loss of accuracy and increase in computational time.

We observe that if g and f are the same mappings (i.e., differ only by the scaling parameter) of a symmetric cross section (a pipe with the axis of zero transverse wake), the step-out wake for the beam on that axis is always $\ln b/a$. However, the transverse wake will always differ by a form factor from the corresponding expression for the transition between round pipes.

The bounding expressions for the longitudinal Green's function Eq.(54) and for the transverse Green's function Eq.(57) can be applied to the exploration of the appropriate transverse beam shape to minimize or maximize the corresponding wake effect.

Appendix A: Evaluation of the cross flux integral

1. Approach 1

We start with the new notation for the conformal mapping function

$$f(\omega, \omega_i) \equiv \chi_i(\omega). \quad (\text{A1})$$

In this section $i, j = 0, s$ and ω_i is the coordinate of the corresponding particle.

We consider the Stock's theorem in a complex plane, that reads

$$\iint_D g dr^2 = \frac{1}{2i} \oint_{\partial D} \int g d\omega^* d\omega. \quad (\text{A2})$$

It holds for an arbitrary complex function g .

Before we may use this formula, we must properly define the integration domain. We cut infinitesimally small circles with a radius r_0 centered on ω_0 and ω_s . We denote

these cut-out areas D_0 and D_s respectively and define the integration domain as : $D = D_{A,B} \setminus (D_0 \cup D_s)$

With Eq.(A1) under Eq.(A2) expression for the exchange integral Eq.(51) gets the following form

$$\begin{aligned} \frac{1}{2i} \oint_{\partial D} \int \left(\frac{\chi'_0 \chi'^*_s}{\chi_0 \chi^*_s} + \frac{\chi'_s \chi'^*_0}{\chi_s \chi^*_0} \right) d\omega^* d\omega = \\ = \frac{1}{2i} \oint_{\partial \tilde{D}'} (\ln \chi^*_s d \ln \chi_0 + \ln \chi^*_0 d \ln \chi_s) \end{aligned} \quad (\text{A3})$$

The integral over $\partial \tilde{D}'$ is a linear combination of integrals over ∂D_0 , ∂D_s and ∂D (see Fig.5a).

First, we evaluate the integral on the contours ∂D_i ($i = 0, s$). On these contours we expand $\chi_i \approx \chi'_i(\omega_i) r_o e^{i\varphi}$, and get:

$$\ln(\chi_i) = \ln |r_0 \chi'_i(\omega_i)| + i\varphi + O(r_0) \quad (\text{A4})$$

$$\ln(\chi_j) = \ln(\chi_j(\omega_i)) + \frac{\chi'_j(\omega_i)}{\chi_j(\omega_i)} r_o e^{i\varphi} + O(r_0)$$

Substitution of this expansion into (A3) gives:

$$\begin{aligned} \frac{1}{2i} \int_{2\pi}^0 \left[\ln(\chi_j(\omega_i)) + \frac{\chi'_j(\omega_i)}{\chi_j(\omega_i)} r_o e^{i\varphi} \right] id\varphi + \\ \frac{1}{2i} \int_{2\pi}^0 [\ln |r_0 \chi'_i(\omega_i)| + i\varphi] \frac{\chi'_j(\omega_i)}{\chi_j(\omega_i)} r_o e^{i\varphi} id\varphi = \\ -\pi \ln(\chi_j(\omega_i)) + O(r_0) \end{aligned} \quad (\text{A5})$$

The integral of ∂D_i is computed in a similar fashion, with the interchange $i \leftrightarrow j$. The remaining integral over ∂D is equal to zero due to the boundary condition Eq.(10).

Combining all together we get the final expression for the exchange integral:

$$I = -\pi \{ \ln [f(\omega_0, \omega_s)] + \ln [f(\omega_s, \omega_0)] \}. \quad (\text{A6})$$

2. Approach 2

To calculate this integral in more rigorous way we introduce new conformal map $\tilde{\chi}_s$ that is based on χ_0

$$\tilde{\chi}_s(\omega) = \frac{\chi_0(\omega_s) - \chi_0(\omega)}{1 - \chi_0(\omega_s) \chi_0(\omega)}. \quad (\text{A7})$$

We treat χ_s as a function of χ_0 and move from integration over $d\omega d\omega^*$ to integration over $d\chi_0 d\chi_0^*$. After we substitute Eq.(A7) and perform a change of variables ($|\partial \chi_0 / \partial \omega|^2 d\omega d\omega^* = d\chi_0 d\chi_0^*$) the integral (51) reads

$$\frac{1}{2i} \oint_{\partial \tilde{D}'} d\chi_0 \int d\chi_0^* \left[\frac{1}{\chi_0} \left(\frac{\tilde{\chi}'_s}{\tilde{\chi}_s} \right)^* + \frac{1}{\chi_0^*} \frac{\tilde{\chi}'_s}{\tilde{\chi}_s} \right]. \quad (\text{A8})$$

Here, the derivative $\tilde{\chi}'_s$ is taken with respect to the variable χ_0 . We substitute $\tilde{\chi}_s$ with the explicit expression

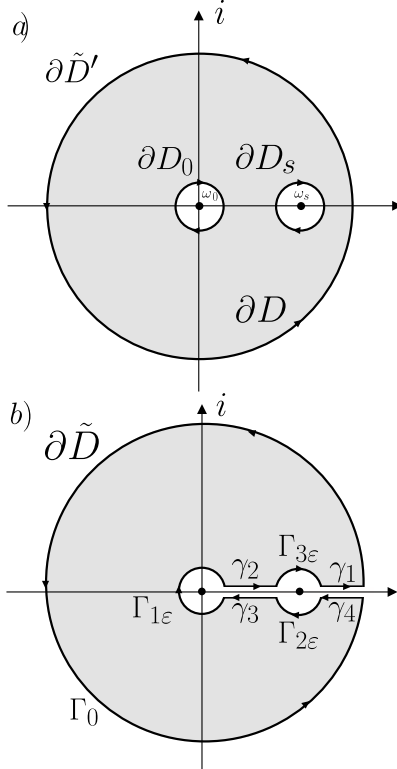


Figure 5. Sketch of the integration contour

and get

$$\frac{1}{2i} \oint_{\partial\tilde{D}'} d\chi_0 \left\{ \frac{1}{\chi_0} [\ln(\chi_0^* - \chi_0(\omega_s)) - \ln(1 - \chi_0^*\chi_0(\omega_s))] + \ln(\chi_0^*) \frac{1 - \chi_0(\omega_s)^2}{(\chi_0(\omega_s) - \chi_0)(1 - \chi_0(\omega_s)\chi_0)} \right\}. \quad (\text{A9})$$

To this end present approach does not differ from the Approach 1. The rigor comes into play now. It is known that the function $\ln(z)$ is not analytic and has a cut in the complex plane. This complicates the evaluation of the integral. To perform this evaluation with care, we introduce the new contour $\partial\tilde{D}$ that is sketched in Fig. 5b.

Integral over $\partial\tilde{D}$ is zero, as the function under integral does not have any singularities or cuts in the region enclosed by the contour. Integration over $\partial\tilde{D}'$ corresponds to the integration over $\Gamma_{1\epsilon} + \Gamma_{2\epsilon} + \Gamma_{3\epsilon} + \Gamma_0$, but this integral equals minus the integral over $\gamma = \gamma_1 + \gamma_2 + \gamma_3 + \gamma_4$. The integral of the contour $\gamma_1 + \gamma_2 + \gamma_3 + \gamma_4$ is evaluated as follows. We introduce the parametrization: on contour $\gamma_1 + \gamma_2 - \chi_0 = x$; on contour $\gamma_1 + \gamma_2 - \chi_0 = xe^{2\pi i}$. With x in the range: $(0; \chi_0(\omega_s) - \epsilon) \cup (\chi_0(\omega_s) + \epsilon; 1)$, but in different directions.

Incorporating everything in Eq.(A9) we get:

$$I = \frac{1 - \chi_0(\omega_s)^2}{2i} v.p. \int_0^1 \frac{2\pi i}{(\chi_0(\omega_s) - x)(\chi_0(\omega_s)x - 1)} dx = -2\pi \ln \chi_0(\omega_s) \quad (\text{A10})$$

This expression is equivalent to

$$I = -\pi [\ln \chi_0(\omega_s) + \ln \chi_s(\omega_0)] \quad (\text{A11})$$

once we recall that $\chi_0(\omega_s) = \tilde{\chi}_s(\omega_0)$. The latter follows from the straightforward substitutions in Eq.(A7).

Appendix B: Connection between magnetic and electric fields

Here we provide a detailed explanation on connection between complex functions that correspond to electric and magnetic fields in Eq.(6) in the cross section of the waveguide, namely $h = ie$.

One can show that Eq.(5) in terms of complex functions Eq.(6) reads

$$\nabla_c^* e = \left(4\pi\rho + \frac{\partial E_z}{\partial \zeta} - i \frac{\partial H_z}{\partial \zeta} \right),$$

$$\nabla_c^* h = i \left(4\pi\rho + \frac{\partial E_z}{\partial \zeta} - i \frac{\partial H_z}{\partial \zeta} \right).$$

Under the assumption of no radiation we get

$$\nabla_c^* e = 4\pi\rho,$$

$$\nabla_c^* h = i4\pi\rho.$$

We introduce operator

$$\nabla_c^* = \frac{\partial}{\partial x} - i \frac{\partial}{\partial y} = 2 \frac{\partial}{\partial \omega} \quad (\text{B1})$$

From Eq.(B1) it is clear that h and ie may differ only by some analytical function $g(w)$.

In order to define this function, we have to examine boundary conditions. We examine PEC waveguide that corresponds to following boundary conditions

$$\mathbf{n} \times \mathbf{E} = 0 \rightarrow \Re[e\tau^*] = 0,$$

$$(\mathbf{n}, \mathbf{H}) = 0 \rightarrow \Im[h\tau^*] = 0.$$

From these conditions we conclude that $g(\omega)$ must to be 0 at the boundary of the waveguide. We recall that $g(\omega)$ is an analytical function and reaches its maximum and minimum at the boundary. From the latter we conclude that $h = ie$.

ACKNOWLEDGMENTS

The author thanks Prof. Donald Marshall of George Washington University for his help with the Zipper algorithm. The work was supported by the Foundation for the Advancement of Theoretical Physics and Mathematics "BASIS" #22-1-2-47-17 and the ITMO Fellowship and Professorship Program.

[1] A. Chao, *Physics of Collective Beam Instabilities in High Energy Accelerators*. Wiley and Sons, New York, 1993.

[2] B. W. Zotter and S. Kheifets, *Impedances and Wakes in High Energy Particle Accelerators*. WORLD SCIENTIFIC, 1998.

[3] K. L. Bane, “Wakefields of sub-picosecond electron bunches,” Tech. Rep. SLAC-Pub-11829, SLAC, 2006.

[4] K.-Y. Ng, “Wake fields in a dielectric-lined waveguide,” *Phys. Rev. D*, vol. 42, pp. 1819–1828, Sep 1990.

[5] A. Tremaine, J. Rosenzweig, and P. Schoessow, “Electromagnetic wake fields and beam stability in slab-symmetric dielectric structures,” *Phys. Rev. E*, vol. 56, pp. 7204–7216, Dec 1997.

[6] S. S. Baturin, I. L. Sheinman, A. M. Altmark, and A. D. Kanareykin, “Transverse operator method for wakefields in a rectangular dielectric loaded accelerating structure,” *Phys. Rev. ST Accel. Beams*, vol. 16, p. 051302, May 2013.

[7] P. D. Hoang, G. Andonian, I. Gadjev, B. Naranjo, Y. Sakai, N. Sudar, O. Williams, M. Fedurin, K. Kusche, C. Swinson, P. Zhang, and J. B. Rosenzweig, “Experimental characterization of electron-beam-driven wake-field modes in a dielectric-woodpile cartesian symmetric structure,” *Phys. Rev. Lett.*, vol. 120, p. 164801, Apr 2018.

[8] M. Aicheler, P. Burrows, M. Draper, T. Garvey, P. Lebrun, K. Peach, N. Phinney, H. Schmickler, D. Schulte, and N. Toge, *A Multi-TeV Linear Collider Based on CLIC Technology: CLIC Conceptual Design Report*. CERN Yellow Reports: Monographs, Geneva: CERN, 2012.

[9] T. Behnke, J. E. Brau, B. Foster, J. Fuster, M. Harrison, J. M. Paterson, M. Peskin, M. Stanitzki, N. Walker, and H. Yamamoto, “The international linear collider technical design report - volume 1: Executive summary,” 2013.

[10] J. Galayda, J. Stohr, Z. Huang, P. Emma, N. H.-D., W. J., M. Rowen, P. Heimann, J. Arthur, J. Albino, R. Chestnut, A. Perazzo, G. Haller, D. Marsh, and S. Rokni, “LCLS-II Conceptual Design Report,” Tech. Rep. SLAC-R-978, SLAC, 2011.

[11] A. Zholents, W. Gai, S. Doran, R. Lindberg, J. Power, N. Strelnikov, Y. Sun, E. Trakhtenberg, I. Vasserman, C. Jing, A. Kanareykin, Y. Li, Q. Gao, D. Shchegolkov, and E. Simakov, “A preliminary design of the collinear dielectric wakefield accelerator,” *Nuclear Instruments and Methods in Physics Research Section A: Accelerators, Spectrometers, Detectors and Associated Equipment*, vol. 829, pp. 190–193, 2016. 2nd European Advanced Accelerator Concepts Workshop - EAAC 2015.

[12] A. Zholents *et al.*, “A Conceptual Design of a Compact Wakefield Accelerator for a High Repetition Rate Multi User X-ray Free-Electron Laser Facility,” in *Proc. 9th International Particle Accelerator Conference (IPAC’18), Vancouver, BC, Canada, April 29-May 4, 2018*, no. 9 in International Particle Accelerator Conference, (Geneva, Switzerland), pp. 1266–1268, JACoW Publishing, June 2018. <https://doi.org/10.18429/JACoW-IPAC2018-TUPMF010>.

[13] A. Siy, N. Behdad, J. Booske, G. Waldschmidt, and A. Zholents, “Design of a cylindrical corrugated waveguide for a collinear wakefield accelerator,” *Phys. Rev. Accel. Beams*, vol. 25, p. 121601, Dec 2022.

[14] A. Siy, N. Behdad, J. Booske, G. Waldschmidt, and A. Zholents, “Electromagnetic design of the transition section between modules of a wakefield accelerator,” *Phys. Rev. Accel. Beams*, vol. 26, p. 012802, Jan 2023.

[15] I. Zagorodnov and T. Weiland, “Te/tm field solver for particle beam simulations without numerical cherenkov radiation,” *Phys. Rev. ST Accel. Beams*, vol. 8, p. 042001, Apr 2005.

[16] J.-L. Vay, D. P. Grote, R. H. Cohen, and A. Friedman, “Novel methods in the particle-in-cell accelerator code-framework warp,” *Computational Science & Discovery*, vol. 5, p. 014019, dec 2012.

[17] G. Stupakov, K. L. F. Bane, and I. Zagorodnov, “Optical approximation in the theory of geometric impedance,” *Phys. Rev. ST Accel. Beams*, vol. 10, p. 054401, May 2007.

[18] K. L. F. Bane, G. Stupakov, and I. Zagorodnov, “Impedance calculations of nonaxisymmetric transitions using the optical approximation,” *Phys. Rev. ST Accel. Beams*, vol. 10, p. 074401, Jul 2007.

[19] S. S. Baturin and A. D. Kanareykin, “Cherenkov radiation from short relativistic bunches: General approach,” *Phys. Rev. Lett.*, vol. 113, p. 214801, Nov 2014.

[20] S. S. Baturin and A. D. Kanareykin, “New method of calculating the wakefields of a point charge in a waveguide of arbitrary cross section,” *Phys. Rev. Accel. Beams*, vol. 19, p. 051001, May 2016.

[21] S. S. Baturin, G. Andonian, and J. B. Rosenzweig, “Analytical treatment of the wakefields driven by transversely shaped beams in a planar slow-wave structure,” *Phys. Rev. Accel. Beams*, vol. 21, p. 121302, Dec 2018.

[22] B. D. O’Shea, G. Andonian, S. S. Baturin, C. I. Clarke, P. D. Hoang, M. J. Hogan, B. Naranjo, O. B. Williams, V. Yakimenko, and J. B. Rosenzweig, “Suppression of deflecting forces in planar-symmetric dielectric wakefield accelerating structures with elliptical bunches,” *Phys. Rev. Lett.*, vol. 124, p. 104801, Mar 2020.

[23] W. Qin, M. Dohlus, and I. Zagorodnov, “Short-range wakefields in an l-shaped corrugated structure,” *Phys. Rev. Accel. Beams*, vol. 26, p. 064402, Jun 2023.

[24] S. A. Heifets and S. A. Kheifets, “Coupling impedance in modern accelerators,” *Rev. Mod. Phys.*, vol. 63, pp. 631–673, Jul 1991.

[25] I. Zagorodnov, “Indirect methods for wake potential integration,” *Phys. Rev. ST Accel. Beams*, vol. 9, p. 102002, Oct 2006.

[26] H. Henke and W. Bruns, “Calculation of wake potentials in general 3D structures,” *Conf. Proc. C*, vol. 060626, pp. 2170–2172, 2006.

[27] W. K. H. Panofsky and W. A. Wenzel, “Some Considerations Concerning the Transverse Deflection of Charged Particles in Radio-Frequency Fields,” *Review of Scientific Instruments*, vol. 27, pp. 967–967, 12 2004.

[28] M. Lavrentiev and B. Shabat, *Methods of Complex Function Theory*. Nauka, Moskow, 1987.

[29] R. A. Silverman, *Introductory Complex Analysis*. Dover Publications, Inc., New York, 1972.

[30] L. Palumbo, V. G. Vaccaro, and M. Zobov, “Wake fields and impedance,” in *CERN Accelerator School: Course on Advanced Accelerator Physics (CAS)*, pp. 331–390, 9

1994.

[31] D. E. Marshall and S. Rohde, “Convergence of a variant of the zipper algorithm for conformal mapping,” *SIAM Journal on Numerical Analysis*, vol. 45, no. 6, pp. 2577–2609, 2007.